

Joint Modeling of Bridge Admittance and Body Radiativity for Efficient Synthesis of String Instrument Sound by Digital Waveguides

Esteban Maestre, Gary P. Scavone, and Julius O. Smith

Abstract—In the context of efficient sound synthesis by digital waveguides, we present a novel methodology for joint modeling of string instrument body radiativity and driving-point bridge admittance functions, as obtained from experimental data. From our modeling framework, aimed at simulation of guitar and bowed string sound, here we focus on the body of the instrument and leave aside the strings. First, a modal decomposition of the measured bridge admittance is obtained by means of a novel frequency-domain algorithm for optimization of recursive digital filters in parallel form. Then, from extracted modal parameters, the radiativity, and admittance functions are modeled by projecting measurements over a common modal basis, enforcing passivity of the two-dimensional admittance model by means of semidefinite programming. We propose a formulation that enables the joint realization of bridge reflectance and sound radiativity as a lumped delay line termination in which a single bank of resonant filters is shared among all string reflection and body radiation outputs. Our approach provides efficient means to model two-dimensional (2-D) bridge reflectance, 2-D string-string coupling, sound radiation with an arbitrary number of outputs, and (implicitly) vibrational energy loss from the bridge transmittance to nonradiating modes and dissipation.

Index Terms—Cello, digital waveguide, fiddle, guitar, modal, optimization, passive, parallel, reflectance, violin, viola.

I. INTRODUCTION

PHYSICAL modeling synthesis refers to a family of techniques for constructing computational models of acoustic musical instruments based on efficient mathematical approximations of the sound-generating physics. Within the different approaches to construct such models, digital waveguides [1]

have been widely used to construct efficient models of string instruments over the last thirty years. In digital waveguide synthesis, string vibration is usually modeled by simulating velocity (or force) wave propagation via delay lines, with low-order digital filters used to account for lumped propagation losses and wave dispersion. It is often the case, however, that the acoustic signature of an instrument is mostly determined by the instrument's body and radiativity properties [2].

String instruments, such as in the guitar and violin families, radiate sound indirectly: energy from thin vibrating strings is transferred to a more efficient radiating body of larger surface area. To a large extent, sound radiation is produced due to the transverse velocity of the instrument body surfaces (e.g., the front or back plates), and such surface motion is transferred to the body through the force that the string exerts on the instrument's bridge. The way in which the input force at the bridge is related to the transverse velocity of the body surfaces depends on very intricate mechanical interactions among the bridge, sound post, front and back plates, air inside the body cavity, etc. [2]–[4]. It is therefore important that, in addition to explicitly representing the string itself, a physically meaningful digital waveguide model incorporates an appropriate representation of the two following processes: first, the relation between the applied force at the bridge and the induced velocity at the bridge, i.e., the bridge input admittance, which leads both to lossy wave reflection from the bridge and to string-string wave coupling; second, the relation between the applied force at the bridge and the sound projected by the body, i.e., the instrument's radiativity.

Due to linearity and time-invariance, it is possible to lump string losses and bridge-admittance losses together in a single high-order filter terminating the delay line for each string vibration plane [5]. However, because the strings are not identical, separate filters must be designed for each string in this formulation. For 2D string motion, two filters must be designed for each string termination, giving a total of 12 filter-designs for a six-string guitar. This approach requires many high-order filters (each separately designed) to model bridge losses that are not inherent in the strings. String losses themselves, on the other hand, can be modeled effectively with very low-order filters [6]–[8], while the body modes “seen” by the strings at the bridge can enjoy a single implementation shared among all the strings. Moreover, an individual-string approach does not preserve beating patterns and natural string-string couplings, and therefore needs additional string-coupling filters or

Manuscript received August 30, 2016; revised January 8, 2017 and March 13, 2017; accepted March 13, 2017. Date of publication March 29, 2017; date of current version April 24, 2017. This work was supported by the European Research Council through a Marie Curie IOF Fellowship. The associate editor coordinating the review of this manuscript and approving it for publication was Prof. Augusto Sarti. (Corresponding author: Esteban Maestre.)

E. Maestre is with the Computational Acoustic Modeling Lab, McGill University, Montréal, QC H3A0G4, Canada, and the Music Technology Group, Universitat Pompeu Fabra, Barcelona 08002, Spain (e-mail: esteban@ccrma.stanford.edu).

G. P. Scavone is with the Computational Acoustic Modeling Lab, McGill University, Montréal, QC H3A0G4, Canada (e-mail: gary.scavone@mcgill.ca).

J. O. Smith is with the Center for Computer Research in Music and Acoustics, Stanford University, Stanford, CA 94305 USA (e-mail: jos@ccrma.stanford.edu).

Color versions of one or more of the figures in this paper are available online at <http://ieeexplore.ieee.org>.

Digital Object Identifier 10.1109/TASLP.2017.2689241

artificial beating models [9], etc., that further reduce the efficiency of the synthesis algorithm. Additionally, a separate filtering component is needed for modeling body radiativity [10], such as by recursive digital filtering with a single [11] or multiple [12] outputs, convolution with measured impulse responses [13], or frequency-domain techniques [14].

Leaving aside the string models, for which several effective modeling methods are available (see, e.g., [5] and the references therein), we present here an experimental framework for using admittance and radiativity measurements to design a single filter structure that efficiently simulates bridge two-dimensional transverse wave reflectance, two-dimensional string-string coupling, sound radiation with an arbitrary number of outputs, and (implicitly) vibrational energy loss from the bridge transmittance to non-radiating modes and dissipation.

A. Prior Work

Possibly the first comprehensive work on efficient digital modeling of violin bridge admittances for sound synthesis was developed in [6], which proposed and evaluated several techniques for automatic design of common-denominator IIR filter parameters from admittance measurements, making real-time violin synthesis an affordable task. However, while efficiency and accuracy can be well accomplished (also when applied to other string instruments [11]), positive-realness (passivity) [15] cannot be easily guaranteed with common-denominator IIR schemes, leaving open the possibility of instability when building string terminations. In that regard, the modal framework [16] offers a twofold advantage: (i) the admittance can be represented by a physically meaningful formulation, and (ii) positive-realness can be guaranteed. The modal framework has been used extensively to study the mechanical properties of violins and other string instruments [2], [17], but only recently it has been applied to synthesizing positive-real bridge driving-point admittances by fitting digital filter coefficients to experimental measurements [18]–[22], which we summarize below.

In a recent inspiring paper, Bank and Karjalainen [18] construct a positive-real (passive) driving-point admittance model of a guitar bridge by combining all-pole modeling and the modal formulation: they first tune parameters of an all-pole IIR filter based on measurement data, and use the roots of the resulting denominator as a basis for a modal synthesis model in which positive-realness is imposed by an artificial constraint at the expense of some reduced accuracy. This method is compared to ours in Section V-A.

Two other relevant works ([17], [23]) use guitar and cello bridge admittance measurements to construct two-dimensional matrices of bridge reflection functions based on the modal framework. Although ignoring radiativity and not focusing on efficient sound synthesis, their wave-based modeling approach informs the development of bridge losses and two-dimensional string-string coupling.

B. This Paper

Extending our previously published works [19]–[22], here we solve a similarly constrained problem, but using the modal

formulation in a modeling process that also incorporates radiativity. The new procedure can be summarized as follows:

- 1) We obtain the system poles from admittance measurements by optimization of a recursive filter in parallel form whose structure matches the discretized version of a modal decomposition,
- 2) we synthesize a passive, driving-point two-dimensional admittance matrix model by finding a projection of the system poles via semidefinite programming,
- 3) we synthesize a radiativity transfer function vector expressed as a projection of the same system poles, and
- 4) we propose an efficient formulation in which string-string coupling bridge reflectance and body radiativity are implemented by means of a shared digital filter.

In more detail, our new method extends our prior work as follows: First, *modal decomposition* and *admittance and radiativity modeling* are now described as separate processes; this makes sense from a physics standpoint and, although they were already differentiated in [21], the first process was vaguely described and no details were given. Second, both mode parametrization and mode optimization algorithms are different from [19]–[21] but inspired by [22], which should be considered as the basic framework used here (optimization of recursive digital filters in parallel form under novel numerator constraints). Third, in this paper we provide a detailed description of how modal parameters are initialized prior to optimization. Fourth, we provide details on how to perform modal parameter initialization and modal decomposition over a warped frequency axis. Finally, the digital resonator structure in the radiativity model has now changed with respect to the *complex gain radiation* model described in [21]: to avoid a DC offset in the radiation output when the bridge force DC offset is non-zero (e.g., when bowing), the radiativity model is now forced to have a zero at DC. This, in turn, makes the whole reflectance and radiativity realizations come out differently relative to [21].

The rest of the paper is organized as follows. Section II provides an overview of our methodology. Section III gives details about the admittance and radiativity measurement procedures employed for this work. Next, in Section IV we describe our optimization approach for modal decomposition from admittance measurements. Sections V and VI respectively present models for admittance and radiativity transfer functions. Finally, in Section VII we propose an efficient joint formulation of bridge reflectance and body radiativity via a single, lumped, string termination.

II. OVERVIEW OF OUR APPROACH

We are interested in constructing efficient, physically inspired models of musical instruments of the guitar and violin families. We aim to design recursive digital filters that accurately represent the string termination as observed from vibration measurements of the string-bridge interaction in real instruments, and the sound radiation efficiency as measured using a microphone. In our sound synthesis framework we model transverse string motion by means of digital waveguides [15], emulating two orthogonal planes of transverse string velocity, and the strings

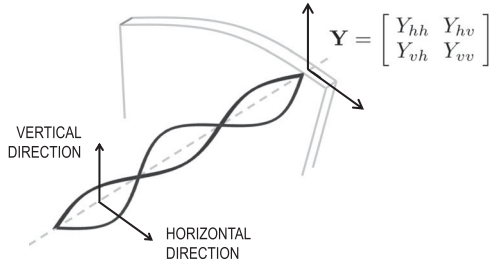


Fig. 1. Two-dimensional driving-point admittance of a violin bridge.

are coupled to the bridge through a 2×2 admittance matrix model. The focus of this work is on modeling of string instrument bodies, rather than the strings themselves. The admittance model, formulated via the modal framework after a modal decomposition obtained from measurements, is used to simulate the mechanical behavior of the body of the instrument. Additionally, we simulate how the instrument body radiates sound via constructing a radiativity model that is formulated as a projection of the same vibration modes that are used to formulate the admittance matrix model.

The *admittance* $Y(\omega) = V(\omega)/F(\omega)$ is a physical frequency response $Y(\omega)$ that maps an applied *force* $F(\omega)$ to the resulting *velocity* $V(\omega) = Y(\omega)F(\omega)$ at each frequency ω in a linear, time-invariant, mechanical structure, where ω denotes frequency in rad/s. A velocity vector $\mathbf{V}(\omega)$ and force vector $\mathbf{F}(\omega)$ at a particular point on the structure are related via the *driving-point admittance matrix* $\mathbf{Y}(\omega)$ by $\mathbf{V}(\omega) = \mathbf{Y}(\omega)\mathbf{F}(\omega)$. In order to emulate transverse wave reflection and transmission at the bridge, we need to construct a digital representation of the two-dimensional matrix

$$\mathbf{Y}(\omega) = \begin{bmatrix} Y_{hh}(\omega) & Y_{hv}(\omega) \\ Y_{vh}(\omega) & Y_{vv}(\omega) \end{bmatrix}, \quad (1)$$

corresponding to the bridge driving-point admittance relating the bridge force vector $\mathbf{F}(\omega) = [F_h(\omega) F_v(\omega)]^T$ and bridge velocity vector $\mathbf{V}(\omega) = [V_h(\omega) V_v(\omega)]^T$ as represented in Fig. 1, where subscripts indicate string (horizontal and vertical) polarizations, and $Y_{hv} = Y_{vh}$ (symmetric admittance). By taking a measurement $\mathbf{Y}(\omega)$ from a real instrument, one can pose this as a system identification problem where a parametric model $\hat{\mathbf{Y}}(\omega)$ is tuned so that an error measure $\varepsilon(\mathbf{Y}(\omega), \hat{\mathbf{Y}}(\omega))$ is minimized. Analogously, a radiativity frequency response

$$\mathbf{E}(\omega) = [E_h(\omega) E_v(\omega)] \quad (2)$$

can be defined to relate the bridge force vector $\mathbf{F}(\omega)$ and the sound pressure scalar $P(\omega)$ at a point in the vicinity of the instrument, leading to $P(\omega) = \mathbf{E}(\omega)\mathbf{F}(\omega)$. Again, from a radiativity frequency response measurement $\mathbf{E}(\omega)$ one can tune a parametric radiativity model $\hat{\mathbf{E}}(\omega)$ by minimization of an error measure $\varepsilon(\mathbf{E}(\omega), \hat{\mathbf{E}}(\omega))$.

Relying on the modal framework, we use an admittance model that serves the purpose of modal decomposition. This modal decomposition is expressed as a basis of vectors that are obtained by evaluating the responses of recursive second-order digital filters, one per mode. Both the admittance and the radiativity

models used for sound synthesis are defined as projections over the same basis of vibration modes, each modeled via one of such filters. The focus of this paper is (i) to provide a comprehensive methodology for constructing digital models of parametric functions $\hat{\mathbf{Y}}(\omega)$ and $\hat{\mathbf{E}}(\omega)$, i.e., digital filters $\hat{\mathbf{Y}}(z)$ and $\hat{\mathbf{E}}(z)$, defined experimentally by fitting their parameters to measured admittance frequency response matrix $\mathbf{Y}(\omega)$ and measured radiativity frequency response vector $\mathbf{E}(\omega)$ respectively; and (ii) to propose a formulation for the realization of said digital filters in the context of realistic, efficient synthesis of string sound by digital waveguides.

A. Admittance Modeling via the Modal Framework

The basic principle of the modal framework is the assumption that a vibrating structure can be modeled by a set of resonant elements satisfying the equation of motion of a damped mass-spring oscillator, each representing a natural mode of vibration of the system. Assuming linearity, the individual responses from the resonant elements (modes) to a given excitation can be summed to obtain the response of the system [24]. In theory, a mechanical structure presents an unbounded number of modes of vibration, and experimental modal analysis techniques allow to find a finite subset of (prominent) modes that best describe the vibrational properties as observed from real measurements in the audio band. In general, admittance analysis via the modal framework begins from surface velocity measurements taken after excitation of the structure with a given force impulse or sweep function.

As introduced in [18], a useful set of structurally passive two-dimensional driving-point admittance matrices can be expressed in the digital domain as

$$\hat{\mathbf{Y}}(z) = \sum_{m=1}^M H_m(z) \mathbf{R}_m, \quad (3)$$

where \mathbf{R}_m is a 2×2 positive semidefinite (nonnegative definite) matrix, and each scalar modal response

$$H_m(z) = \frac{1 - z^{-2}}{(1 - p_m z^{-1})(1 - p_m^* z^{-1})} \quad (4)$$

is a second-order resonator determined by a pair of complex conjugate poles p_m and p_m^* . The numerator $1 - z^{-2}$ is the bilinear-transform image of s -plane zeros at DC and infinity, respectively, arising under the “proportional damping” assumption [25], [34]. It can be checked that $H_m(z)$ is positive real for all $|p_m| < 1$ (stable poles). Since the admittance model $\hat{\mathbf{Y}}(z)$ is positive real (passive) whenever the gain matrices \mathbf{R}_m are positive semidefinite, the passive bridge-modeling problem can be posed as finding poles p_m and positive-semidefinite gain matrices \mathbf{R}_m such that some error measure is minimized.

In the work by Bank and Karjalainen [18], poles from an all-pole IIR time-domain fit are used as the modal basis to estimate \mathbf{R}_m . Once the poles have been estimated from measurement data, they find matrices \mathbf{R}_m as follows: First, they independently solve three one-dimensional linear projection problems, each corresponding to an entry in the upper triangle of matrix \mathbf{Y} . This leads to three length- M modal gain vectors. Then, since simply

rearranging such gain vectors as a set of M independent 2×2 symmetric gain matrices (matrices \mathbf{R}_m of (3)) does not enforce passivity (all of the \mathbf{R}_m need to be positive semidefinite), they ensure passivity by computing the spectral decomposition of each \mathbf{R}_m , and recompose each matrix after setting to zero any negative eigenvalues.

In our work, as outlined in the next subsection and detailed through Sections IV and V, we take a different approach for pole finding and admittance modeling. The first difference is that we find poles by optimizing the coefficients of a digital filter structure that more exactly matches the admittance model, as opposed to first relying on all-pole modeling and then reusing obtained poles to model admittance. The second difference is that, instead of ensuring passivity by discarding negative eigenvalues of individual matrices \mathbf{R}_m , we propose a formulation that allows to use convex optimization to find all matrices \mathbf{R}_m at once while enforcing passivity. In Section V-A we provide a numerical example in which we compare the results obtained with the method of [18] to those obtained with our method.

B. Method Summary

To support the reader in following the rest of the paper, we provide here a brief summary of our method. As introduced before, the models for driving-point bridge admittance and body radiativity presented in this work are defined as projections over a common basis of vibrational modes whose frequencies and bandwidths are extracted from experimental data.

Both the modal decomposition and the admittance and radiativity modeling are performed from velocity and sound pressure response measurements taken from real instruments while exciting the bass-side bridge corner with an impact hammer in two orthogonal directions, namely the *horizontal* and *vertical* directions of transverse motion of the strings. Regarding admittance, three measurements are obtained for each instrument, leading to the three frequency responses that form the upper diagonal of the matrix of (1). In terms of radiativity, two measurements are obtained for each instrument, leading to the pair of frequency responses appearing in (2).

The first and most important step is to perform modal decomposition from the admittance measurements. Our assumption here is that all M relevant modes of vibration that will form the common basis are observable from the diagonal entries of the admittance measurement matrix. Following this assumption, modal decomposition is performed via iterative, constrained optimization of the position of poles of a digital filter in parallel form, whose response is matched against the diagonal entries of the measured admittance at each iteration.

Once the M modes have been estimated, we proceed with modeling admittance and radiativity. For the admittance, we first construct a basis of M frequency responses, each corresponding to the digital resonator of (4) as defined by the m -th vibration mode. Then we use semidefinite programming to project the frequency-domain admittance measurement matrix onto the basis of frequency responses and find gain matrices \mathbf{R}_m of (3) while imposing that all \mathbf{R}_m be positive semidefinite. For the radiativity we construct a different basis, still obtained from the

same set of M modes, and solve a projection problem to model each of the frequency responses of (2).

Finally, we propose an efficient, joint realization of bridge reflectance and body radiativity models that relies on a sole, shared digital filter in which parallel sections are shared among all reflectance and radiativity outputs.

III. MEASUREMENTS

In a hemi-anechoic chamber, we carried out admittance and radiativity measurements on three decent quality bowed string instruments (violin, viola, cello) from the Schulich School of Music at McGill University, and also on a steel string acoustic guitar by Godin. The instruments were held vertically, with the neck pointing up. Cushioned clamps were used to rigidly hold all instruments from the neck, with the low end of the body resting on a foam cushion impeding their free motion during the measurements. In order to damp the low-frequency vibrational modes of the holding structure, sandbags were conveniently placed at different locations on the metal stands. Rubber bands were used to damp the strings.

The impact hammer, which has been long used in the context of acoustic analysis or modeling for sound synthesis [6], [10], [26], [27], provides a simple and effective method to excite the bridge of stringed instruments with great repeatability. For our measurements, a calibrated impact hammer was used to excite the corner of the bass side of the bridge in two orthogonal directions corresponding to the horizontal and vertical directions of the transverse motion of the strings. Simultaneously to the hammer force, the bridge edge surface velocity was measured by means of a laser Doppler vibrometer aimed at a point located as close as possible to the hammer, and the radiated sound was measured by means of two omnidirectional microphones facing the top plate, placed 1 meter away from the instrument. In our modeling framework the strings meet at a single point representing a common driving-point admittance of the bridge, so for practical matters, we could also have chosen to measure on the treble side. We chose to measure on the bass-bar side because of the higher efficiency of the bridge in driving the top plate, as observed from previous experimental studies of violin acoustics [28]. For consistency, we chose the bass side of the guitar bridge as well. The locations and orientations of the impact hammer, the vibrometer laser beam, and the microphones are schematically illustrated in Fig. 2 for the case of the bowed strings, but it also applies to the guitar. We used a PCB Piezotronics 086E80 miniature impact hammer, a Polytec LDV-100 vibrometer, and two Brüel and Kjaer 4150 measurement microphones. All signals were digitized by means of a National Instruments USB-4431 signal acquisition board. Time-domain signals of force, velocity, and sound pressure were collected, delay-compensated, and stored before using frequency-domain deconvolution for obtaining admittance and radiativity frequency responses. For each of the frequency responses, several measurements were collected and averaged in order to use coherence as a means for selecting the most consistent set. For each instrument, we obtained five frequency responses, all of them sampled at 44.1 kHz: three responses respectively corresponding to the three entries Y_{hh} ,

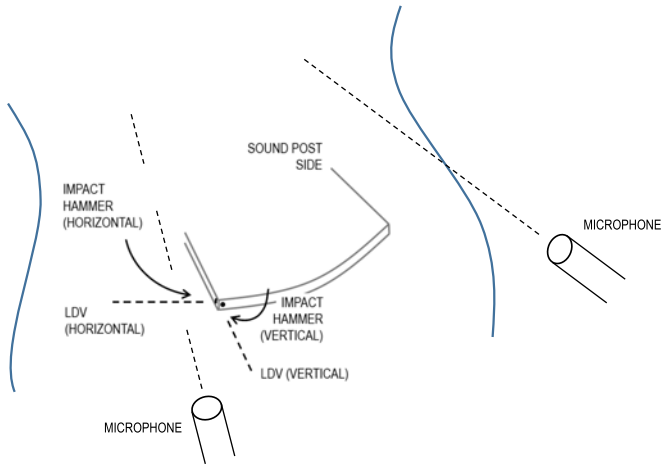


Fig. 2. Schematic illustration of a violin bridge admittance and radiativity measurement using a calibrated impact hammer, and a Laser Doppler Vibrometer (LDV), and two microphones.

Y_{vv} , and Y_{hv} of the bridge driving-point symmetric admittance matrix, and two radiativity measurements E_h and E_v per microphone, respectively corresponding to radiated sound due to horizontal and vertical bridge force.

Dashed-line curves in Fig. 5 show the magnitude frequency responses of admittance measurements Y_{hh} , Y_{vv} , and Y_{hv} , and radiativity measurements E_h and E_v (one microphone) performed on all four instruments, for $80 \leq f \leq 6000$ Hz, where signature and radiating modes exist. This frequency region also corresponds to the region where measurement coherence was consistently high. The first observable radiating mode can be observed around 300 Hz, 260 Hz, 100 Hz, and 200 Hz for the violin, viola, cello, and guitar respectively. Admittance responses show in general little noise, except for some regions of the guitar and cello: for the guitar, Y_{hh} approximately in the region $600 \leq f \leq 1000$, where admittance magnitude is very low, and also in the far low frequency region due to interaction with the vibration modes of the measurement setup (this also happened for the cello in the region below 80 Hz, not displayed); for the cello, the admittance was difficult to measure consistently in the high frequency region (around 4–6 kHz). With respect to radiativity, regions below the first radiation mode always feature a 1/f noise floor above any relevant radiativity information, mainly due to the fact the room was not anechoic.

IV. MODAL DECOMPOSITION

For each instrument, we obtain a modal decomposition by automatic analysis of the bridge driving-point admittance matrix measurements. The process consists of two steps. First, an initial estimation of modes, comprising a set of frequencies and corresponding bandwidths, is performed by processing of spectral peaks in each diagonal term of the measurement matrix, respectively corresponding to the one-dimensional admittances $Y_{hh}(\omega)$ and $Y_{vv}(\omega)$. Then, mode parameters are optimized via a frequency-domain filter design algorithm that uses sequential quadratic programming to minimize the error between measured frequency responses and synthesized frequency responses.

Finally, modal parameters coming from fitting both $Y_{hh}(\omega)$ and $Y_{vv}(\omega)$ are merged into one set of parameters before a final optimization is performed.

A. Initialization Procedure

Obtaining an initial estimation of modal parameters is carried out from the admittance measurement frequency response. The process comprises two main stages: peak selection (leading to modal frequency estimation) and graphical estimation of bandwidths. In the first stage, a finite set of M_L spectral peaks is selected as to represent the resonances corresponding to the M_L modes to be used for modeling the low-frequency region (f_L^-, f_L^+), and M_H broader resonances are included to model the high frequency region (f_H^-, f_H^+). The low and high frequency regions are defined arbitrarily. The selection of the M_L low-frequency resonance peaks is carried out via an iterative procedure by which admittance maxima in (f_L^-, f_L^+) are rated and sorted by a peak salience descriptor computed from a smoothed version of the magnitude response, while the resonances for the high-frequency region are distributed uniformly over (f_H^-, f_H^+). In the second stage, graphical estimation of the M_L modal bandwidths of the low-frequency region is carried out by using the resonance *half-power* rule for each individual peak.

1) *Peak Salience Estimation for Low-Frequency Modes:* A peak salience descriptor t_n is computed for every local maximum ϱ_n found in a smoothed version of the magnitude spectrum of the measured admittance, within (f_L^-, f_L^+). Smoothing is performed via low-pass filtering of the magnitude response when expressed in a logarithmic amplitude scale. Salience estimation is carried out from the log-magnitude admittance spectrum $\Upsilon(f) = \log_{10} |Y(f)|$ as follows. First, for every maximum ϱ_n at frequency f_n , two adjacent minima ϑ_n^- and ϑ_n^+ are respectively found as the absolute minima in the regions (f_{n-1}, f_n) and (f_n, f_{n+1}) respectively. Then, from each n -th pair of adjacent minima $\{\vartheta_n^-, \vartheta_n^+\}$ at respective frequencies f_n^- and f_n^+ , the minimum ϑ_n^* presenting higher log-magnitude is selected, and its log-magnitude value Υ_n^* is used in the computation of the n -th peak salience descriptor t_n as

$$t_n = \int_{f_n^-}^{f_n^+} \Psi_n(f) \Upsilon(f) df, \quad (5)$$

with $\Psi_n(f)$ defined as

$$\Psi_n(f) = \begin{cases} 0 & \text{if } \Upsilon(f) < \Upsilon_n^*, \\ 1 & \text{if } \Upsilon(f) \geq \Upsilon_n^*. \end{cases} \quad (6)$$

2) *Resonance Frequency Estimation for Low-Frequency Modes:* The selection of M_L low-frequency peaks from the magnitude spectrum as corresponding to the resonances of the M_L individual modes to be modeled in the region (f_L^-, f_L^+) is carried out in three steps, involving the use of computed peak saliences.

First, N maxima ϱ_n are found in the region (f_L^-, f_L^+) of $\Upsilon(f)$, with $N > M_L$. For each n -th peak, its salience t_n is computed as described above. From computed saliences, the

M_L peaks presenting higher salience are stored into an array \mathbf{c} of mode candidates, discarding the remaining $N - M_L$ peaks. In a second step, the mode candidate array \mathbf{c} is repopulated by adding a subset of the peaks discarded in the previous selection: for every pair $\{\varrho_{m_L}, \varrho_{m_L+1}\}$ of peaks in \mathbf{c} , the discarded peaks that lay in (f_{m_L}, f_{m_L+1}) are stored into an array \mathbf{d} , from which the peak with highest salience is added to the mode candidate array \mathbf{c} . Finally, assuming that through repopulation Q peaks (with $Q < M_L$) have been added to the mode candidate array \mathbf{c} , $M_L + Q$ salience descriptors are again computed from peaks in \mathbf{c} . After that, the M_L peaks with highest salience in \mathbf{c} are kept, leading to a first estimate of the M_L mode natural frequencies. The repopulation step can be carried out iteratively until array \mathbf{c} remains unchanged, leading to the set of initial estimates for modal frequencies $\mathbf{f} = \{f_1 \dots f_{m_L} \dots f_{M_L}\}$.

3) *Estimation of Bandwidths of Low-Frequency Modes:* From the initial mode frequencies \mathbf{f} , the computation of an initial estimate of the respective bandwidths $\boldsymbol{\beta} = \{\beta_1 \dots \beta_{m_L} \dots \beta_{M_L}\}$ is carried out graphically as follows. For each maximum ϱ_{m_L} located at frequency f_{m_L} , a pair $\{\vartheta_{m_L}^-, \vartheta_{m_L}^+\}$ of adjacent minima is found at frequencies $\{f_{m_L}^-, f_{m_L}^+\}$ by searching for the absolute minimum values of $\Upsilon(f)$ in regions (f_{m_L-1}, f_{m_L}) and (f_{m_L}, f_{m_L+1}) respectively. The segments $J_{m_L}^-(f)$ and $J_{m_L}^+(f)$, corresponding to $\Upsilon(f)$ in regions $(f_{m_L}^-, f_{m_L})$ and $(f_{m_L}, f_{m_L}^+)$ respectively, are linearly approximated to obtain $\hat{J}_{m_L}^-(f) = a_{m_L}^- f + b_{m_L}^-$ and $\hat{J}_{m_L}^+(f) = a_{m_L}^+ f + b_{m_L}^+$. From these two approximations, the steepest slope a_m^* is chosen as $a_{m_L}^* = \max(|a_{m_L}^-|, |a_{m_L}^+|)$ and, by using the *half-power* rule relating the bandwidth and characteristic frequency of a resonator [15], the bandwidth is approximated as $\beta_{m_L} = 3/10 a_{m_L}^*$.

B. Optimization Algorithm

The algorithm used to refine the initial estimation of modal frequencies and bandwidths is based on constrained optimization of the poles of a recursive digital filter in parallel form. In the following, and throughout this subsection, $\hat{H}(z)$ can refer to either of the two diagonal entries of the admittance matrix. The digital filter model is

$$\hat{H}(z) = \sum_{m=1}^M H_m(z) r_m, \quad (7)$$

where each $H_m(z)$ is defined in (4) by a pair of complex-conjugate stable poles, and scalar gains r_m are real. Initial modal frequencies and bandwidths are first expressed in the digital domain by the position of M complex-conjugate pole pairs inside the unit circle: initial mode frequencies f_m are converted to z -plane pole angles via $2\pi f_m / f_s = \angle p_m$, with f_s being the sampling frequency; initial mode bandwidths are converted to z -plane pole radia via $\beta_m = -\log |p_m| / \pi$. Then we employ a gradient descent routine in which, at each i -th step, an objective error function is successively evaluated by projecting a target frequency response over a basis of frequency responses defined by the pole positions at the i -th step. The optimization routine is devised as an adaptation of the filter design technique proposed

in [22], where a set of linear constraints are imposed to enforce feasibility and to aid convergence.

To apply the algorithm for optimizing pole positions by attending to any of the positive-real transfer functions forming the diagonal elements of the admittance matrix, we pose the problem as

$$\begin{aligned} & \underset{\mathbf{w}, \mathbf{s}}{\text{minimize}} && \varepsilon(H, \hat{H}) \\ & \text{subject to} && \mathbf{C}, \end{aligned} \quad (8)$$

where $\varepsilon(H, \hat{H})$ is an error measure between the measured frequency response H and a synthetic frequency response \hat{H} obtained from pole positions as defined by parameter sets \mathbf{w} , \mathbf{s} ; and \mathbf{C} is a set of linear constraints employed to ensure feasibility and to aid convergence. To solve this problem we use sequential quadratic programming [29].

1) *Mode Parametrization:* We parametrize the initial set of M modes by representing each respective m -th complex pole pair in terms of its angle parameter $w_m = |\angle p_m|$ and its radius parameter $s_m = -\log(1 - |p_m|)$. This leads to two parameter sets: a set $\mathbf{w} = \{w_1 \dots w_M\}$ of angle parameter values, and a set $\mathbf{s} = \{s_1 \dots s_M\}$ of radius parameter values. Then, a key step is to sort the pole parameter sets so that linear constraints can be defined in a straightforward manner to ensure that the arrangement of poles inside the unit circle is preserved during optimization, therefore reducing the number of crossings over local minima. Elements in sets \mathbf{w} and \mathbf{s} are jointly sorted as pairs (each pair corresponding to a complex-conjugate pole) by ascending angle parameter w_m .

2) *Constraint Definition:* Constraints \mathbf{C} are defined as follows. First, feasibility is ensured by $0 \leq s_m \forall m \in [1, M]$ and $0 \leq w_m \leq \pi \forall m \in [1, M]$. Second, to aid convergence we constrain the pole sequence order in set \mathbf{w} to be respected, so that all poles appear in ascending angle parameter. This is expressed by $w_{m-1} < w_m < w_{m+1} \forall m \in [2, M-1]$. Moreover, assuming that initialization provides an already trusted first solution, we can bound the search to a region around the initial pole positions. This can be expressed via the additional inequalities $w_m^- < w_m < w_m^+ \forall m \in [1, M]$ and $s_m^- < s_m < s_m^+ \forall m \in [1, M]$, where ‘-’ and ‘+’ superscripts are used to respectively indicate lower and upper bounds, defined during initialization.

3) *Error Computation:* For the optimization routine to successfully approximate the error gradient, we must supply a procedure to evaluate the error function $\varepsilon(H, \hat{H}|_i)$ at step i as a function of the model parameters $\mathbf{w}|_i$ and $\mathbf{s}|_i$ at step i . This is carried out in two steps. First, from the pole positions at iteration i , we solve the convex sub-problem

$$\begin{aligned} & \underset{\mathbf{r}}{\text{minimize}} && \|\hat{\mathbf{H}}|_i \mathbf{r} - \mathbf{h}\|^2 \\ & \text{subject to} && \mathbf{r} \geq 0, \end{aligned} \quad (9)$$

where $\mathbf{r} = [r_1 \dots r_m \dots r_M]^T$ is a vector containing positive gains r_m from (7) to impose positive realness, $\mathbf{h} = [h_1 \dots h_k \dots h_K]^T$ is a vector containing K samples of the measured frequency response H evaluated at K uniformly distributed frequencies $0 \leq \omega_k < \pi$, and $\hat{\mathbf{H}}|_i$ is a matrix of basis

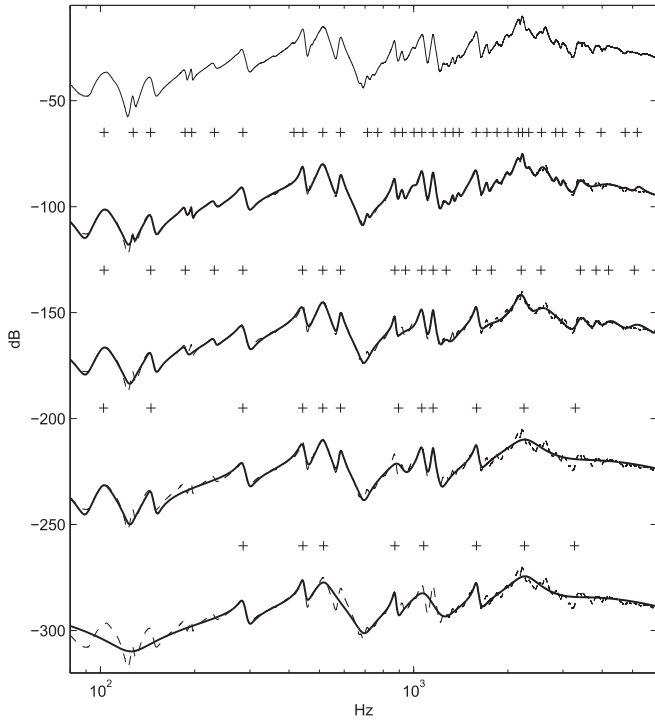


Fig. 3. Example models for the horizontal admittance Y_{hh} of the violin, for different values of M in $80 \leq f \leq 6000$ Hz. The top plot corresponds to the measurement, while each of the remaining four plots (scaled for clarity) display the model (solid curve) superimposed to the measurement (dashed line), together with a depiction of the mode frequencies ('+' symbols). Model orders were, from top to bottom, $M = 36, 24, 14, 9$.

vectors constructed as $\hat{\mathbf{H}}|_i = [\hat{\mathbf{h}}_1|_i \cdots \hat{\mathbf{h}}_m|_i \cdots \hat{\mathbf{h}}_M|_i]$, with each $\mathbf{h}_m|_i = [h_{m,1}|_i \cdots h_{m,k}|_i \cdots h_{m,K}|_i]^T$ containing K samples of the frequency response of $H_m(z)|_i$ evaluated at K uniformly distributed frequencies $0 \leq \omega_k < \pi$, i.e., $h_{m,k}|_i = H_m(e^{j\omega_k})|_i$.

Once the subproblem has been solved, the frequency response of the model $\hat{H}(e^{j\omega})|_i$ at iteration i is obtained as $\hat{\mathbf{H}}|_i \mathbf{r}$, with samples arranged in a vector $\hat{\mathbf{h}}|_i = [\hat{h}_1|_i \cdots \hat{h}_k|_i \cdots \hat{h}_K|_i]^T$ that is used to compute the logarithmic error measure

$$\varepsilon(H, \hat{H}|_i) = \sum_{k=1}^K \left| \log_{10} |\hat{h}_k|_i - \log_{10} |h_k| \right|. \quad (10)$$

We employ a logarithmic error measure to equally account for low-magnitude and high-magnitude regions of the frequency response, so that the parameters of low-amplitude modes are faithfully estimated.

In Fig. 3 we show example models obtained by the optimization algorithm to approximate the one-dimensional admittance Y_{hh} of the violin, for different orders, in $80 \leq f \leq 6000$. Optimizations were performed on a warped frequency axis, for a warping parameter $\lambda = 0.85$, as described in Section IV-D.

C. Modal Decomposition Procedure

The procedure for modal decomposition is described here. The process, making use of the proposed initial estimation and optimization algorithms (Sections IV-A and IV-B respectively), involves three steps.

1) *One-Dimensional Decomposition*: First, two individual modal decompositions are performed from the diagonal entries Y_{hh} and Y_{vv} of the admittance measurement matrix. Each of these two decompositions comprises two estimation steps: first, an initial estimation of modal parameters; second, an optimized estimation of modal parameters. This leads to a set of M_0 modal parameter pairs $\{\omega_{h,m}, \beta_{h,m}\}$ for the horizontal direction and a set of M_0 modal parameter pairs $\{\omega_{v,m}, \beta_{v,m}\}$ for the vertical direction, with each pair defining the m -th modal frequency and corresponding bandwidth.

2) *Mode Merging*: Since many of the modes of the system get excited both in the horizontal and vertical directions, the same mode may likely be estimated from both measurements. Joining the two sets of M_0 modes independently obtained through the individual decompositions as described above leads to a set of $2M_0$ mode candidates from which mode pairs in close proximity to one another can be assumed as corresponding to the same mode of the system and therefore merged. We merge the $2M_0$ mode estimations into a set of M modes (with $M \leq 2M_0$) by means of clustering mode frequencies: from each of M found clusters, we keep only the mode that is closest to the cluster centroid.

3) *Final Estimation*: To obtain the final set of modes that will form the basis, we use a modified version of the optimization algorithm described in Section IV-B. Starting from the set of M modes obtained after merging, we minimize the error measure $\varepsilon_2(\mathbf{Y}, \hat{\mathbf{Y}}) = \varepsilon(Y_{hh}, \hat{Y}_{hh}) + \varepsilon(Y_{vv}, \hat{Y}_{vv})$, where each term in the sum is computed as defined in (10) and accounts for the error between one of the diagonal entries of the admittance matrix and its approximation as a projection over the modal basis defined by mode parameters at step i .

D. Warped Frequency Decomposition

Both initial estimation and optimization of modal parameters can be performed over a warped frequency axis as follows. Our choice for frequency-warping is the bilinear conformal map, which is defined by the all-pass substitution

$$z \leftarrow \frac{\zeta + \lambda}{1 + \lambda\zeta} \quad (11)$$

and takes the unit circle in the z -plane to the unit circle in the ζ -plane in such a way that, for $0 < \lambda < 1$, low frequencies are stretched and high-frequencies are compressed, as in a transformation from frequency in Hertz to a warped, perceptually motivated frequency scale [30], [31]. Warping of measured admittance responses is performed by attending to the phase response of the all-pass transfer function of (11), which leads to a relation between linear frequency ω and warped frequency ϖ that can be realized by spline interpolation.

During initialization (see Section (IV-A)), modal frequencies and bandwidths are estimated over the axis ϖ of warped frequencies. We de-warp initial estimations of frequencies and bandwidths as follows. From each m -th pair of warped mode parameters (i.e., frequency and bandwidth) we first obtain the corresponding complex-conjugate warped pole (pair), represented by ρ_m . From the warped pole, we obtain its linear counterpart

p_m via (11) by

$$p_m = \frac{\rho_m + \lambda}{1 + \lambda \rho_m}, \quad (12)$$

which then leads to linear-frequency mode parameters.

With respect to the optimization procedure (see Section (IV-B)), the parallel nature of the model makes it straightforward to work on a warped frequency axis. Mapping of $H_m(z)$ in (4) to the ζ -plane yields

$$H_m(\zeta) = \gamma_m \frac{1 - \zeta^{-2}}{(1 - \rho_m \zeta^{-1})(1 - \rho_m^* \zeta^{-1})}, \quad (13)$$

where

$$\gamma_m = \frac{1 - \lambda^2}{1 - 2\lambda|p_m| \cos \angle p_m + \lambda^2|p_m|^2}. \quad (14)$$

With this formulation, optimization and modal decomposition are carried out on the ϖ -axis as described in Sections IV-B and IV-C. From optimized, warped-frequency modal parameters we obtain their linear-frequency counterparts again via (12) as described above.

V. ADMITTANCE MODELING

The admittance is modeled by the two-dimensional projection of (3). To guarantee passivity, the problem of finding the projection coefficients is posed as the constrained minimization

$$\begin{aligned} & \underset{\mathbf{R}_m}{\text{minimize}} && \varepsilon(\mathbf{Y}, \hat{\mathbf{Y}}) \\ & \text{subject to} && \mathbf{R}_m \succeq 0 \end{aligned} \quad (15)$$

where the 2×2 matrices \mathbf{R}_m are real and $\varepsilon(\mathbf{Y}, \hat{\mathbf{Y}})$ is an error measure between the measurement and the model. From a two-dimensional admittance measurement (symmetric) matrix \mathbf{Y} , let \mathbf{y}_{hh} , \mathbf{y}_{hv} , and \mathbf{y}_{vv} be column vectors each containing K samples of its respective frequency response, i.e., $y_{hh,k} = Y_{hh}(\omega_k)$, $y_{hv,k} = Y_{hv}(\omega_k)$, $y_{vv,k} = Y_{vv}(\omega_k)$, with $0 \leq \omega_k \leq \pi$. This leads to a $2K \times 2$ matrix of the form

$$\mathbf{Y} = \begin{bmatrix} \mathbf{y}_{hh} & \mathbf{y}_{hv} \\ \mathbf{y}_{hv} & \mathbf{y}_{vv} \end{bmatrix}. \quad (16)$$

Now we proceed with rewriting the right-side of (3) in matrix form as constructed from a projection over the individual modal responses $H_m(e^{j\omega_k})$ with $0 \leq \omega_k \leq \pi$. First, we define a $K \times M$ matrix \mathbf{H} as $\mathbf{H} = [\mathbf{h}_1 \cdots \mathbf{h}_m \cdots \mathbf{h}_M]$, where each \mathbf{h}_m is a column vector with K samples $H_m(e^{j\omega_k})$ in $0 \leq \omega_k \leq \pi$. With matrix \mathbf{H} , we construct a $2K \times 2M$ block-diagonal matrix \mathbf{B} defined as

$$\mathbf{B} = \begin{bmatrix} \mathbf{H} & \mathbf{0} \\ \mathbf{0} & \mathbf{H} \end{bmatrix}, \quad (17)$$

which can be interpreted as a two-dimensional modal response basis. The next step is to set up a $2M \times 2M$ block-symmetric matrix \mathbf{R} as

$$\mathbf{R} = \begin{bmatrix} \mathbf{R}_{hh} & \mathbf{R}_{hv} \\ \mathbf{R}_{hv} & \mathbf{R}_{vv} \end{bmatrix}, \quad (18)$$

where \mathbf{R}_{hh} , \mathbf{R}_{hv} , and \mathbf{R}_{vv} are $M \times M$ diagonal, real matrices. In the m -th entry of the diagonal of matrix \mathbf{R}_{hh} appears the coefficient from entry (1, 1) of the individual projection matrix \mathbf{R}_m in (3). Analogously, matrix \mathbf{R}_{hv} will contain coefficients from the M entries (1, 2), and \mathbf{R}_{vv} from entries (2, 2). Now, with modal basis \mathbf{B} and projection matrix \mathbf{R} , it is possible to express the model frequency response matrix as $\hat{\mathbf{Y}} = \mathbf{BRS}$, where

$$\mathbf{S} = \begin{bmatrix} \mathbf{1} & \mathbf{0} \\ \mathbf{0} & \mathbf{1} \end{bmatrix} \quad (19)$$

acts as a $2M \times 2$ summation matrix, with each $\mathbf{1}$ representing a length- M vector of ones. It is important to note that $\mathbf{R} \succeq 0 \Leftrightarrow \mathbf{R}_m \succeq 0 \forall m \in [1, M]$, implying that the model $\hat{\mathbf{Y}}$ will be passive if matrix \mathbf{R} is positive semidefinite. Now we are ready to express problem (15) as a matrix norm minimization problem that includes a positive semidefinite constraint on matrix \mathbf{R} . If expressing the model approximation error as $\varepsilon(\mathbf{Y}, \hat{\mathbf{Y}}) = \|\mathbf{Y} - \mathbf{BRS}\|$, the problem can be written as

$$\begin{aligned} & \underset{\mathbf{R}}{\text{minimize}} && \|\mathbf{Y} - \mathbf{BRS}\| \\ & \text{subject to} && \mathbf{R} \succeq 0, \end{aligned} \quad (20)$$

which is convex and can be solved via semidefinite programming by means of CVX, a package for specifying and solving convex programs [32].

Frequency responses of example admittance models, obtained on a warped frequency axis for $\lambda = 0.8$ while constraining mode frequencies to be below 10 kHz, are shown in Fig. 5. We can observe how the models tend to perform slightly better at approximating the diagonal terms Y_{hh} and Y_{vv} . For the particular case of the guitar, it is clear how the model does a better job at approximating the vertical term, mostly due to the fact that horizontal admittance of the guitar presents significantly lower energy, especially in $600 \leq f \leq 1000$.

A. Comparison to Bank and Karjalainen's Method

To compare our admittance modeling method to that proposed by Bank and Karjalainen [18], we used a 2D violin bridge admittance measurement to obtain two models, one for each method. In both cases the order was set to $M = 32$, and pole (mode) finding was performed on the warped domain, with $\lambda = 0.75$. Results are shown in Fig. 4. Two main reasons are behind the improvement showed by our method. The first reason is pole estimation. We believe that using an all-pole model (as in [18]) to estimate the poles of a pole-zero system (the admittance) is, in principle, less effective than using a pole-zero model (the one proposed here). Moreover, being able to initialize or constrain pole positions to be within an interest region helps in controlling the desired resolution. The second reason is passive enforcement. In our method passivity is guaranteed at the time of estimating the gains via formulating a convex problem which, from a mathematical perspective, provides a better suited and more elegant framework for joint estimation of all gain matrices at once. Conversely, the method of [18] is to first solve three problems independently and then prune the solution by discarding non-passive gain components, leading to a loss of accuracy

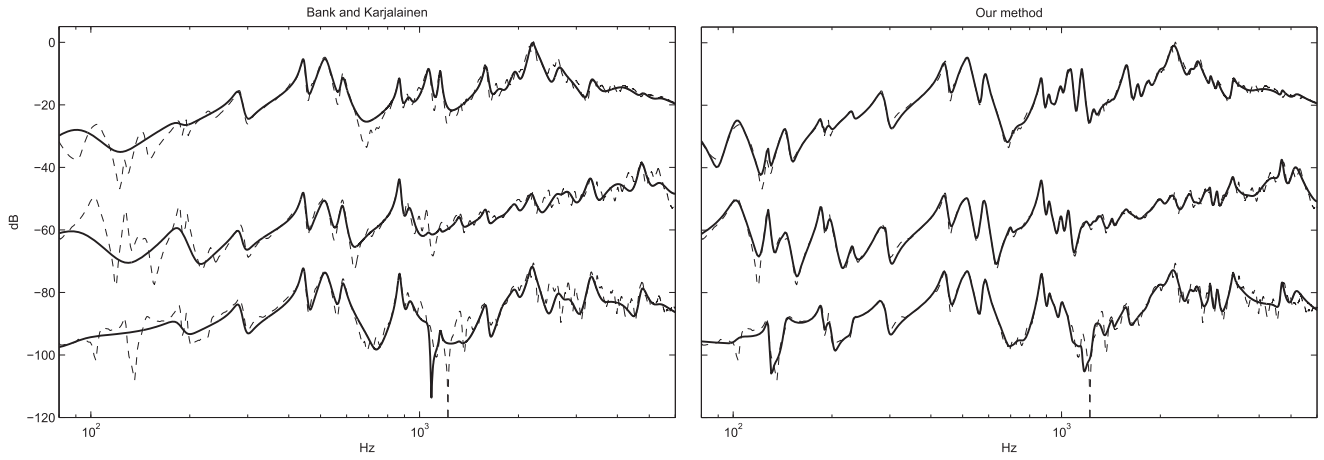


Fig. 4. Comparison results for a violin admittance matrix. Frequency responses of admittance models with order $M = 32$ and warping coefficient $\lambda = 0.75$, displayed for $80 \leq f \leq 6000$ Hz. Admittance response curves correspond, from top to bottom, to Y_{hh} , Y_{vv} , and Y_{vh} . Dashed lines are used for measurements, while solid lines are used for models. For clarity, Y_{vv} and Y_{vh} responses were scaled by -30 dB and -60 dB respectively.

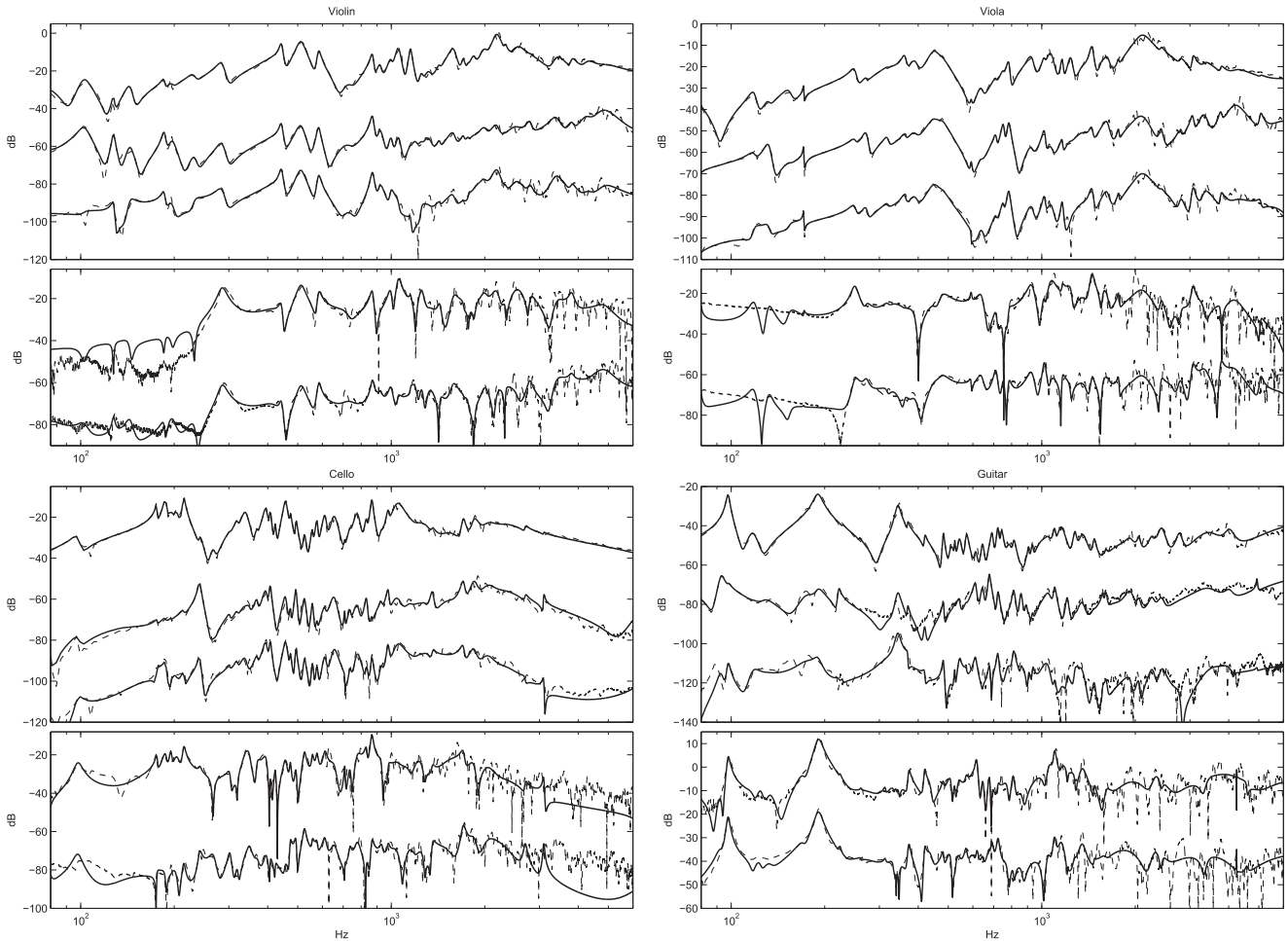


Fig. 5. Frequency responses of admittance models (top plot) and radiation models (bottom plot) for $M = 36$, displayed for $80 \leq f \leq 6000$ Hz. Admittance response curves correspond, from top to bottom, to Y_{hh} , Y_{vv} , and Y_{vh} . Radiativity response curves correspond, from top to bottom, to E_h and E_v . Dashed lines are used for measurements, while solid lines are used for models. For clarity, responses were scaled as follows: for the violin, viola, and cello, Y_{vv} and Y_{vh} were scaled by -30 dB and -60 dB respectively; for the guitar, Y_{vv} and Y_{vh} were scaled by -50 dB and -70 dB respectively; E_v were scaled by -40 dB in all cases.

caused by a preventive downscaling of mode amplitudes: in particular for this example, we found 18 (out of 64) negative eigenvalues when enforcing passivity.

VI. RADIATIVITY MODELING

Measured radiativity frequency responses are $E_h(\omega)$ and $E_v(\omega)$, for horizontal and vertical bridge excitation respectively. Our assumption is that the total sound pressure at the microphone will be the sum of the radiated contributions from the two directions (horizontal and vertical) of the bridge force excitation. Our aim is to construct a digital filter $\hat{\mathbf{E}}(z)$ such that the sound pressure signal $P(z)$ can be obtained during synthesis as

$$P(z) = \hat{\mathbf{E}}(z)\mathbf{F}(z). \quad (21)$$

We model the two scalar transfer functions of $\hat{\mathbf{E}}(z)$ as projections over the modal basis. We first define each m -th radiativity modal (basis) function $U_m(z)$ as

$$U_m(z) = \frac{1 - z^{-1}}{(1 - p_m z^{-1})(1 - p_m^* z^{-1})}, \quad (22)$$

which corresponds to a two-pole resonator with one added zero at DC. We chose to use this basis so that the resonator structure matches that of the admittance model. Now, we express either of the radiativity scalar transfer functions $E_h(z)$ or $E_v(z)$ in $\hat{\mathbf{E}}(z)$ as

$$\hat{E}(z) = \sum_{m=1}^M (e_{0,m} + e_{1,m} z^{-1}) U_m(z), \quad (23)$$

where $e_{0,m}$ and $e_{1,m}$ are real-valued coefficients that allow control of both the amplitude and the phase of the resonator.

Given K samples of the target radiativity frequency response $E(\omega)$ and the set of M complex-conjugate pole pairs $\mathbf{p} = \{p_1 \cdots p_m \cdots p_M\}$ defining the modal basis, let vectors $\mathbf{e}_0 = [e_{0,1} \cdots e_{0,m} \cdots e_{0,M}]^T$ and $\mathbf{e}_1 = [e_{1,1} \cdots e_{1,m} \cdots e_{1,M}]^T$ contain numerator coefficients in (23). Projection coefficients can be obtained via least-squares by

$$\underset{\mathbf{e}}{\text{minimize}} \|\mathbf{B}\mathbf{e} - \mathbf{d}\|^2, \quad (24)$$

where $\mathbf{e} = [\mathbf{e}_0^T \ \mathbf{e}_1^T]^T$ is a real-valued vector; \mathbf{d} contains K uniformly distributed samples of the target frequency response at frequencies $0 \leq \omega_k < \pi$, i.e., $d_k = E(\omega_k)$; and \mathbf{B} is a $K \times 2M$ matrix of basis functions constructed as $\mathbf{B} = [\mathbf{u}_{0,1} \cdots \mathbf{u}_{0,m} \cdots \mathbf{u}_{0,M} \ \mathbf{u}_{1,1} \cdots \mathbf{u}_{1,m} \cdots \mathbf{u}_{1,M}]$ with column vectors defined as follows: each vector $\mathbf{u}_{0,m} = [u_{0,m,1} \cdots u_{0,m,k} \cdots u_{0,m,K}]^T$ contains K uniformly distributed samples of $U_m(e^{j\omega})$ at frequencies $0 \leq \omega_k < \pi$, i.e., $u_{0,m,k} = U_m(e^{j\omega_k})$; and similarly vector $\mathbf{u}_{1,m} = [u_{1,m,1} \cdots u_{1,m,k} \cdots u_{1,m,K}]^T$ contains K frequency-domain samples $u_{1,m,k} = e^{-j\omega_k} U_m(e^{j\omega_k})$.

Frequency responses of example radiativity models, obtained on a warped frequency axis for $\lambda = 0.8$, are displayed in Fig. 5. In general, radiativity profiles are well approximated above the first radiating mode. As expected, models show better accuracy in the vertical direction for the guitar, and in the horizontal direction for the bowed string instruments. In particular for the

cello, the approximation of radiativity profiles is worse in the high frequencies. Increasing error at high frequencies is typical in acoustic modeling. In our case, not using a fully anechoic chamber and not hanging the instruments could be a source for such error. In fact, from our measurements we cannot determine whether the radiativity resonances in the high-frequency region correspond to *actual* modes of the instrument, or are instead caused by the *non ideal* environment. Thus, the error can be expected because only admittance measurements are used to perform the modal decomposition, and there are many unresolved high-frequency modes in these measurements that determine important details of the high-frequency radiativity. Fortunately, due to decreasing frequency-resolution at higher frequencies in human hearing, statistical models can suffice at high frequencies, so that only crude reflected (at the bridge) and transmitted (bridge-to-air) power measurements may be needed for a psychoacoustically adequate model.

VII. EFFICIENT REALIZATION

Following the digital waveguide formulation for loaded junctions [15], let $\mathbf{v}_s^+(n)$ and $\mathbf{v}_s^-(n)$ respectively be the vectors of incoming and outgoing transversal velocity waves (in our case, each vector is two-dimensional) from the s -th string connected to the bridge. Analogously, let $\mathbf{f}_s^+(n)$ and $\mathbf{f}_s^-(n)$ be the vectors of incoming and outgoing transversal force waves of the s -th string acting on the bridge. The transversal velocity $\mathbf{v}_s(n)$ and force $\mathbf{f}_s(n)$ of the n -th string at the bridge are $\mathbf{v}_s(n) = \mathbf{v}_s^+(n) + \mathbf{v}_s^-(n)$ and $\mathbf{f}_s(n) = \mathbf{f}_s^+(n) + \mathbf{f}_s^-(n)$.

Being a series connection for transverse waves, the bridge and the endpoints of the S strings present the same velocity at all times, while the total sum of string forces must equal that of the bridge. This yields $\mathbf{v}(n) = \mathbf{v}_1(n) = \dots = \mathbf{v}_S(n)$ and $\mathbf{f}(n) = \sum_{s=1}^S \mathbf{f}_s(n)$, with $\mathbf{v}(n)$ and $\mathbf{f}(n)$ being the bridge velocity and force vectors respectively. In the z -domain, it can be proved that

$$\mathbf{F}(z) = \frac{2 \sum_{s=1}^S \mathbf{Z}_s \mathbf{V}_n^+(z)}{1 + \mathbf{Z}_T \mathbf{Y}(z)}, \quad (25)$$

where \mathbf{Z}_s is a diagonal matrix representing the wave impedance of the s -th string, $\mathbf{Z}_T = \sum_{s=1}^S \mathbf{Z}_s$, and $\mathbf{Y}(z)$ is the z -domain expression for the model of the driving-point admittance. From the bridge force vector $\mathbf{F}(z)$, it should be straightforward to compute the bridge velocity vector $\mathbf{V}(z)$ via

$$\mathbf{V}(z) = \mathbf{Y}(z)\mathbf{F}(z). \quad (26)$$

Back in the time domain, from the bridge velocity vector $\mathbf{v}(n)$ it is possible to obtain the outgoing velocity wave vectors by means of $\mathbf{v}_s^-(n) = \mathbf{v}(n) - \mathbf{v}_s^+(n)$.

Because the formulation of the bridge driving-point admittance $\mathbf{Y}(z)$ presents a parallel structure that we want to maintain in our implementation, inverting $\mathbf{Y}(z)$ as it appears in (25) is impractical (the parallel structure would be lost). This problem could be overcome by reformulating each scalar modal response $H_m(z)$ in a similar fashion as proposed in [33] and later applied in [18], where wave-digital parallel adaptors were used to interconnect multiple string (waveguide) terminations. Here we propose a compact formulation that provides three advantages:

(i) it enables the direct attachment of any number of waveguide terminations without the need of wave-digital parallel adaptors; (ii) it allows obtaining both the bridge velocity and the bridge force as intermediate signals during computation of the reflected waves; and (iii) it facilitates the efficient computation of any number of radiation outputs without the need for extra second-order sections.

First, we rewrite the admittance model in (3) as

$$\mathbf{Y}(z) = (1 + z^{-1}) \sum_{m=1}^M U_m(z) \mathbf{R}_m, \quad (27)$$

where each scalar $U_m(z)$ is

$$U_m(z) = \frac{1 - z^{-1}}{1 + a_{1,m} z^{-1} + a_{2,m} z^{-2}}, \quad (28)$$

with $a_{1,m} = -2|p_m| \cos(\angle p_m)$ and $a_{2,m} = |p_m|^2$. Now, we rewrite each scalar $U_m(z)$ as $U_m(z) = 1 + z^{-1} U_m^q(z)$, with

$$U_m^q(z) = \frac{c_{0,m} + c_{1,m} z^{-1}}{1 + a_{1,m} z^{-1} + a_{2,m} z^{-2}}, \quad (29)$$

where $c_{0,m} = -1 - a_{1,m}$ and $c_{1,m} = -a_{2,m}$. With this formulation, $\mathbf{Y}(z)$ can be written as

$$\mathbf{Y}(z) = (1 + z^{-1})(\mathbf{X} + z^{-1} \mathbf{X}^q(z)), \quad (30)$$

where

$$\mathbf{X} = \sum_{m=1}^M \mathbf{R}_m, \quad \mathbf{X}^q(z) = \sum_{m=1}^M U_m^q(z) \mathbf{R}_m. \quad (31)$$

Now we use (25), (26), and (30) to derive the two z -domain expressions needed for our reflectance model:

$$\mathbf{F}(z) = \frac{2 \sum_{n=1}^N \mathbf{Z}_n \mathbf{V}_n^+(z) - z^{-1} \mathbf{R}(z)}{1 + \mathbf{Z}_T \mathbf{X}} \quad (32)$$

$$\mathbf{V}(z) = (1 + z^{-1}) \mathbf{X} \mathbf{F}(z) + z^{-1} (1 + z^{-1}) \mathbf{X}^q(z) \mathbf{F}(z), \quad (33)$$

where $\mathbf{R}(z) = (\mathbf{X} + (1 + z^{-1}) \mathbf{X}^q(z)) \mathbf{Z}_T \mathbf{F}(z)$.

For the radiativity realization, we take advantage of the fact that the bridge force vector $\mathbf{F}(z)$ is available as an intermediate step. We first rewrite each transfer function $E(z)$ from $\mathbf{E}(z)$ in (21) as

$$E(z) = \sum_{m=1}^M e_{0,m} U_m(z) + \sum_{m=1}^M e_{1,m} z^{-1} U_m(z) \quad (34)$$

where $e_{0,m}$ and $e_{1,m}$ are real. Following, we express $E(z)$ as

$$E(z) = E_0 + z^{-1} E_1 + z^{-1} E_0^q(z) + z^{-2} E_1^q(z), \quad (35)$$

where

$$E_0 = \sum_{m=1}^M e_{0,m}, \quad E_1 = \sum_{m=1}^M e_{1,m}, \quad (36)$$

$$E_0^q(z) = \sum_{m=1}^M U_m^q(z) e_{0,m}, \quad E_1^q(z) = \sum_{m=1}^M U_m^q(z) e_{1,m}. \quad (37)$$

Now, it is possible to obtain the sound pressure signal $P(z)$ as

$$P(z) = (\mathbf{E}_0 + z^{-1} \mathbf{E}_1 + z^{-1} \mathbf{E}_0^q(z) + z^{-2} \mathbf{E}_1^q(z)) \mathbf{F}(z), \quad (38)$$

where $\mathbf{E}_0 = [E_{0,h} \ E_{0,v}]$, $\mathbf{E}^1 = [E_{1,h} \ E_{1,v}]$, $\mathbf{E}_0^q(z) = [E_{0,h}^q(z) \ E_{0,v}^q(z)]$, and $\mathbf{E}_1^q(z) = [E_{1,h}^q(z) \ E_{1,v}^q(z)]$ all present horizontal and vertical components. It is important to note that the respective direction terms in $\mathbf{X}^q(z)$, $\mathbf{E}_0^q(z)$, and $\mathbf{E}_1^q(z)$ share inputs and parallel structure: all four m -th scalar terms $U_m^q(z)$ present in each of the direction components (horizontal or vertical) of (32), (33), and (37) can be implemented as one common second-order section fed with the corresponding bridge force direction component, irrespective of the number of radiativity outputs.

VIII. CONCLUSION

The proposed method is able to produce admittance and radiation models that efficiently simulate the behavior of the instruments with great accuracy within the region of interest between 80 Hz and 6 KHz, where signature radiating modes appear. Because of inherent limitations of the employed instrumentation, measured responses outside the interest range showed low coherence. In particular for the cello and the guitar, the interaction between modes of the measurement apparatus and lower-frequency modes of the instrument made measuring and modeling a more difficult task. For the admittance models, it is important to include the lower frequency region (i.e., between 0 and 80 Hz) in the fitting process. This allows the modes of the measurement apparatus (prominent peaks below 80 Hz) to also be modeled, leading to a more consistent overall estimation that accounts for the interaction of such modes with the *actual* modes of the instrument. Once the estimation is finished, those modes and their respective gain matrices can be discarded. In general, both accuracy and convergence times are improved if carrying out the estimation on a warped frequency axis.

Example sounds, including one-pole filters to simulate string losses, are available online.¹ Plucked string (radiated) sounds for guitar, violin, viola, and cello open strings were obtained by using reflectance and radiation models as described in the paper, with $M = 36$, and two radiation outputs for stereo rendering. In all four cases, ideal plucks are recreated by string velocity initialization.

A potential improvement to the fitting method can be obtained by embedding the semidefinite programming step as part of an outer loop in which mode parameters are estimated, although it would imply a higher computational cost. A perceptual evaluation might be needed to confirm improvements. Another issue to be resolved is that, in some cases, modal decompositions obtained from admittance measurements do not lead to modal bases able to accurately represent the radiation profiles in the high end (see the cello radiativity models in Fig. 5). A solution to this problem could be worked out by also accounting for the radiation patterns within the modal fitting step, but, as we discussed at the end of Section VI, in our case it is nearly impossible to determine whether those resonances correspond to *actual* body modes. In fact, high overlap in the high frequencies should make modal fitting increasingly difficult in the high end; luckily, the decreasing frequency-resolution at higher

¹<http://ccrma.stanford.edu/~esteban/suppl/taslp2016>

frequencies in human hearing might indeed compensate for that effect. Further analyses could encourage the construction of statistical admittance and radiation models, where modal frequencies, bandwidths, and amplitudes follow empirically inferred distributions. Multi-microphone radiation measurements would lead to obtaining per-mode directional patterns, expressed as a function of the numerator coefficients in the radiativity model. This, in turn, could be used to construct a spherical modal basis with which one could efficiently treat virtual instruments as three-dimensional volumetric sources in virtual acoustic environments.

REFERENCES

- [1] J. O. Smith, "Physical modeling using digital waveguides," *Comput. Music J.*, vol. 16, no. 4, pp. 74–91, 1992.
- [2] T. Rossing, *The Science of String Instruments*. New York, NY, USA: Springer-Verlag, 2010.
- [3] L. Cremer, *The Physics of the Violin*. Cambridge, MA, USA: MIT Press, 1984.
- [4] N. H. Fletcher and T. D. Rossing, *The Physics of Musical Instruments*, 2nd ed. New York, NY, USA: Springer-Verlag, 1998.
- [5] B. Bank and V. Välimäki, "Robust loss filter design for digital waveguide synthesis of string tones," *IEEE Signal Process. Lett.*, vol. 10, no. 1, pp. 18–20, Jan. 2003.
- [6] J. O. Smith, "Techniques for digital filter design and system identification with application to the violin," Ph.D. dissertation, Dept. Elect. Eng., Stanford University, Stanford, CA, USA, 1983.
- [7] M. Karjalainen, V. Välimäki, and Z. János, "Towards high-quality sound synthesis of the guitar and string instruments," in *Proc. Int. Comput. Music Conf.*, 1993, pp. 56–63.
- [8] V. Välimäki and T. Tolonen, "Development and calibration of a guitar synthesizer," *J. Audio Eng. Soc.*, vol. 46, no. 9, pp. 766–778, Sep. 1998 (also in Proceedings of the 103rd Convention of the Audio Engineering Society, New York, NY, USA, Sep. 1997).
- [9] J. Rauhala, M. Laurson, V. Välimäki, H. Lehtonen, and V. Norilo, "A parametric piano synthesizer," *Comput. Music J.*, vol. 32, no. 4, pp. 17–30, 2008.
- [10] G. Bissinger, "Structural acoustics model of the violin radiativity profile," *J. Acoust. Soc. Amer.*, vol. 124, no. 6, pp. 4013–4023, 2008.
- [11] M. Karjalainen and J. O. Smith, "Body modeling techniques for string instrument synthesis," in *Proc. Int. Comput. Music Conf.*, 1996.
- [12] B. Bank, "Direct design of parallel second-order filters for instrument body modeling," in *Proc. Int. Comput. Music Conf.*, 2007, pp. 458–465.
- [13] C. Desvages and S. Bilbao, "Two-polarisation physical model of bowed strings with nonlinear contact and friction forces, and application to gesture-based sound synthesis," *Appl. Sci.*, vol. 6, no. 5, 2016, Art. no. 135.
- [14] A. Pérez-Carrillo, J. Bonada, V. Välimäki, A. Bucci, and J. Pätynen, "Non-impulsive signal deconvolution for computation of violin sound radiation patterns and applications in sound synthesis," *J. Acoust. Soc. Amer.*, vol. 130, no. 2, pp. 1020–1029, 2011.
- [15] J. O. Smith, *Physical Audio Signal Processing*. Stanford, CA, USA: W3K Publishing, 2004. [Online]. Available: <http://ccrma.stanford.edu/jos/pasp/>
- [16] K. D. Marshall, "Modal analysis of a violin," *J. Acoust. Soc. Amer.*, vol. 77, no. 2, pp. 695–709, 1985.
- [17] J. Woodhouse, "Plucked guitar transients: Comparison of measurements and synthesis," *Acta Acustica United Acustica*, vol. 90, no. 5, pp. 945–965, 2004.
- [18] B. Bank and M. Karjalainen, "Passive admittance matrix modeling for guitar synthesis," in *Proc. Int. Conf. Digit. Audio Effects*, 2010.
- [19] E. Maestre, G. P. Scavone, and J. O. Smith, "Modeling of a violin input admittance by direct positioning of second-order resonators," in *Proc. 162nd Meeting Acoust. Soc. Amer.*, 2011.
- [20] E. Maestre, G. P. Scavone, and J. O. Smith, "Digital modeling of bridge driving-point admittances from measurements on violin-family instruments," in *Proc. Stockholm Music Acoust. Conf.*, 2013, pp. 101–108.
- [21] E. Maestre, G. P. Scavone, and J. O. Smith, "Digital modeling of string instrument bridge reflectance and body radiativity for sound synthesis by digital waveguides," in *Proc. IEEE Workshop Appl. Signal Process. Audio Acoust.*, 2015.
- [22] E. Maestre, G. P. Scavone, and J. O. Smith, "Design of recursive digital filters in parallel form by linearly constrained pole optimization," *IEEE Signal Process. Lett.*, vol. 23, no. 11, pp. 1547–1550, Nov. 2016.
- [23] H. Mansour, J. Woodhouse, and G. P. Scavone, "Enhanced wave-based modeling of musical strings. Part 1: Plucked strings," *Acta Acustica United Acoust.*, vol. 102, no. 6, pp. 1082–1093, 2016.
- [24] J. M. Adrien, "The missing link: Modal synthesis," in *Representations of Musical Signals*, G. D. Poli, A. Piccialli, and C. Roads, Eds. Cambridge, MA, USA: MIT Press, 1991, pp. 269–298.
- [25] J. Rayleigh, *The Theory of Sound*, vol. 1. New York, NY, USA: Macmillan, 1877.
- [26] E. V. Jansson, "Admittance measurements of 25 high quality violins," *Acta Acustica United Acustica*, vol. 83, no. 2, pp. 337–341, 1997.
- [27] C. Saitis, C. Fritz, B. L. Giordano, and G. P. Scavone, "Bridge admittance measurements of 10 preference-rated violins," in *Proc. Acoust. 2012 Nantes Conf.*, 2012.
- [28] J. Alonso and E. V. Jansson, "Input admittance, eigenmodes, and quality of violins," in *Proc. 103rd Meeting Acoust. Soc. Amer.*, 1982, pp. 60–75.
- [29] J. Nocedal and S. J. Wright, *Numerical Optimization*. New York, NY, USA: Springer-Verlag, 2006.
- [30] J. O. Smith and J. S. Abel, "Bark and ERB bilinear transforms," *IEEE Trans. Speech Audio Process.*, vol. 7, no. 6, pp. 697–708, Nov. 1999.
- [31] A. Härmä, M. Karjalainen, L. Savioja, V. Välimäki, U. K. Laine, and J. Huopaniemi, "Frequency-warped signal processing for audio applications," *J. Audio Eng. Soc.*, vol. 48, no. 11, pp. 1011–1031, 2000.
- [32] S. Boyd and L. Vandenberghe, *Convex Optimization*. Cambridge, U.K: Cambridge Univ. Press, 2004. [Online]. Available: <http://www.stanford.edu/boyd/cvxbook/>
- [33] M. Karjalainen, "Efficient realization of wave digital components for physical modeling and sound synthesis," *IEEE Trans. Audio, Speech, Lang. Process.*, vol. 16, no. 5, pp. 947–956, Jul. 2008.
- [34] J. Rayleigh, *The Theory of Sound*, vol. 2. New York, NY, USA: Macmillan, 1878.

Esteban Maestre received the B.Sc. and M.Sc. degrees in electrical engineering from Universitat Politècnica de Catalunya, Barcelona, Spain, in 2000 and 2003, respectively, and the D.E.A. and Ph.D. degrees in computer science and digital communication from Universitat Pompeu Fabra, Barcelona, in 2006 and 2009, respectively. From 2001 to 2006, he was a Lecturer at Universitat Politècnica de Catalunya. He was a Junior Researcher at Philips Research Laboratories, Aachen, Germany, during 2003 and 2004. From 2004 to 2013, he was a Researcher (Music Technology Group) and a Lecturer (Department of Information and Communication Technologies) at Universitat Pompeu Fabra. He carried out postdoctoral research at the Center for Computer Research in Music and Acoustics, Stanford University, between 2008 and 2014. Between 2012 and 2013, he was a Visiting Researcher in the Department of Applied Math, Universidad Federico Santa María, Santiago, Chile. Through a Marie Curie IOF Fellowship, he is currently with the Computational Acoustics Modeling Lab/Center for Interdisciplinary Research in Music Media and Technology, McGill University.

Gary P. Scavone received the B.Sc. and B.A. degrees in electrical engineering and music from Syracuse University, NY, USA, respectively, and the M.Sc. and Ph.D. degrees in electrical engineering and music from Stanford University, Stanford, CA, USA. He is an Associate Professor of Music Technology at McGill University, Montreal, QC, Canada, where he directs the Computational Acoustic Modeling Laboratory. His research interests include acoustic modeling, analysis and synthesis of musical systems, and sound synthesis software development.

Julius O. Smith received the B.S.E.E. degree in control, circuits, and communication from Rice University, Houston, TX, USA, in 1975 and the M.S. and Ph.D. degrees in electrical engineering from Stanford University, Stanford, CA, USA, in 1978 and 1983, respectively. His Ph.D. research was devoted to improved methods for digital filter design and system identification applied to music and audio systems. From 1975 to 1977, he was with the Signal Processing Department, ESL, Sunnyvale, CA, on systems for digital communications. From 1982 to 1986, he was with the Adaptive Systems Department, Systems Control Technology, Palo Alto, CA, where he worked in the areas of adaptive filtering and spectral estimation. From 1986 to 1991, he was at NeXT Computer, Inc., responsible for sound, music, and signal processing software for the NeXT computer workstation. After NeXT, he became an Associate Professor in the Center for Computer Research in Music and Acoustics, Stanford, teaching courses and pursuing research related to signal processing techniques applied to music and audio systems. Continuing this work, he is currently a Professor of music and (by courtesy) electrical engineering at Stanford University. For more information, see <http://ccrma.stanford.edu/~jos/>.